Systematic study of kinematic and dynamic moments of inertia of superdeformed bands with N_pN_n scheme

Honey Sharma[1] Neha Sharma[2] H. M. Mittal[1;1)]

[1] Dr. B.R. Ambedkar National Institute of Technology, Jalandhar, 144011, India
[2] CT Institute of Engineering Management and Technology, Jalandhar, 144020, India

Abstract: The systematics of kinematic moment of inertia $J^{(1)}$ and dynamic moment of inertia $J^{(2)}$ of superdeformed (SD) bands in $A\sim130$, 150, 190 mass regions have been studied. We have obtained the values of $J^{(1)}$ and $J^{(2)}$ for all the SD bands observed in the $A\sim130$, 150, 190 mass regions by using the experimental intraband E2 transition energies. The result of this work includes the variation of $J^{(1)}$ with the product of valence proton and neutron numbers (N_pN_n). The phenomenon of band mixing has been observed in the $A\sim130$, 150 mass regions and band crossing has been observed in the $A\sim190$ mass region. The systematics also includes the variation of $J^{(2)}$ with the product of valence proton and neutron numbers (N_pN_n). Evidence of staggering behaviour has been observed in all three $A\sim130$, 150 and 190 mass regions. We present for the first time the variation of $J^{(1)}$ and $J^{(2)}$ of SD bands in the $A\sim130$, 150, 190 mass regions with N_pN_n.

Keywords: kinematic moment of inertia $J^{(1)}$, dynamic moment of inertia $J^{(2)}$, N_pN_n scheme

PACS: 21.90.+f, 27.60.+j, 27.70.+q **DOI:** 10.1088/1674-1137/41/8/084104

1 Introduction

The main factor which helps in the development of nuclear structure is the p-n interaction, which was noticed earlier by Shalit and Goldhaber [1]. Talmi [2] observed that the p-n interaction is the primary cause for deformed nuclei. Federman and Pittel [3–5] and Federman and Campos [6] emphasized the significance of the p-n interaction between nucleons in spin partner orbits, which results in the rapid phase transition near the $A=100$ mass region. Casten [7, 8] proposed a simple quantity called N_pN_n (the product of valence proton number N_p and valence neutron number N_n) which is used for estimating the residual proton and neutron and helps in the evolution of nuclear deformation [1, 3, 9]. A simple pattern is observed when nuclear data disclosing the nuclear deformation is plotted against the N_pN_n scheme [7]. Many theoretical studies provide an insight into the nuclear structure by examining the collectivity in nuclei using the N_pN_n scheme. Casten [7] highlighted the importance of the p-n interaction in explaining the nuclear structure, phase transitions and collectivity by plotting the variation of N_pN_n with nuclear observables for the $A\sim100-200$ mass region. Further information in this regard is provided by the p- factor parameter introduced by Casten [10]. The properties of nuclei far from the stability line for three mass regions $A\sim100$, 150, 190 are also explained by the concept of the N_pN_n scheme. Casten [7, 11] also explains the smooth variation of N_pN_n with energy systematics of even-even nuclei in different mass regions.

Several other theorists have also studied the vital role of p-n interactions in the framework of the N_pN_n scheme. Zhang et al. [12] suggested a method to calculate p-n interaction energies for individual protons and neutrons. A linear behaviour has also been observed between p-n interaction strength against N_pN_n. Gupta et al. [13, 14] examined the systematic dependence of the $\gamma-g$ interband B(E2) ratios on the N_pN_n product and suggested the shape phase transition of the 2_1^+ state depends on total boson number N_B and N_pN_n product. Subsequently, Gupta et al. [15] proposed a power law expression for a single term and analysed the variation of a parameter with N, Z and N_pN_n for the nuclei in the $A=150-200$ mass region. Saini and Gupta [16] studied the variation of softness parameter with N_pN_n by using the VMI NSP model. In the same year, Gupta and Kavathekar [17] found the relationship between rotational energy and N_pN_n, showing that the rotational energy increases with the increase of N_pN_n. Zhao et al. [18] applied the N_pN_n scheme to the even-even nuclei and the same scheme worked well for odd-even, even-odd and doubly- odd nuclei. Zhao and Arima [19] implemented the N_pN_n scheme to non-yrast levels of even-even nuclei

Received 25 January 2017, Revised 17 April 2017

1) E-mail: mittal.hm@lycos.com

and found new types of structural evolution for higher excitations.

Jin et al. [20] proposed an empirical formula for the lowest excitation energy of 2^+ states in even-even nuclei with N_pN_n. Byun et al. [21] explained the concept of the N_pN_n scheme and proton-neutron interactions. Fu et al. [22] obtained the correlation between integrated p-n interactions by using binding energies and N_pN_n with respect to the doubly closed nucleus. Recently, the systematic dependence of Grodzin product on N_pN_n was studied by Kumari and Mittal [23]. Some impressive outcomes appeared when the N_pN_n scheme was applied over the SD bands. Mittal and Sharma [24] calculated the $\pm$Fo values of the SD bands for the $72 \leqslant N \leqslant 82$ region and studied the behaviour of $\pm$Fo values with the N_pN_n scheme. Sharma and Mittal [25] also studied the nuclear softness parameter with N_pN_n and suggested that the superdeformed (SD) bands are more rigid than normal deformed (ND) bands.

The moment of inertia of the nucleus depends on the pairing correlation [26]. The pairing correlation is much weaker in SD bands than in ND bands [27]. The pairing becomes weak in SD bands because all the pairs of nucleons are destroyed by the Coriolis force. Therefore, their spins get aligned along the rotational axis when the rotational frequency is increased [26]. However, when $J^{(1)}$ is plotted versus rotational frequency and $J^{(2)}$ versus rotational frequency for the $A \sim 130$, 150 mass regions, both $J^{(1)}$ and $J^{(2)}$ decrease with increasing rotational frequency. This is because the pairing is strongly suppressed by the Coriolis force and the anti- pairing effect of deformation in the $A \sim 130$, 150 mass regions. The decrease of the values of $J^{(1)}$ and $J^{(2)}$ with increasing rotational frequency can further be explained by high N intruder occupation quantum numbers (intruder orbitals) [28]. In the $A \sim 190$ mass region, when $J^{(1)}$ is plotted versus rotational frequency and $J^{(2)}$ versus rotational frequency, both $J^{(1)}$ and $J^{(2)}$ increase with increasing rotational frequency. This also leads to weaker pairing, but in the $A \sim 190$ mass region pairing still plays a vital role due to small deformations. The increase in $J^{(1)}$ and $J^{(2)}$ with the increase in rotational frequency can also be explained by the combined alignment of both high N quasi− protons and quasi- neutrons [29]. The variation of $J^{(1)}$ and $J^{(2)}$ with rotational frequency behaves differently in different mass regions $A \sim 130$, 150 and 190. Therefore, the above facts motivate us to study the variations of $J^{(1)}$ and $J^{(2)}$ with N_pN_n and their behaviour in the $A \sim 130$, 150 and 190 mass regions.

$J^{(1)}$ and $J^{(2)}$ are important quantities for nucleus characterization. $J^{(1)}$ is a spin-dependent quantity which shows an appreciable change with orbital alignment, deformation-driving effects, mass and pairing [30]. Therefore, it becomes interesting to observe the variation of $J^{(1)}$ with other observables. $J^{(2)}$ is a quantity which can be deduced even in the absence of spin and it varies strongly from one nucleus to another [30]. The value of $J^{(2)}$ also helps in providing information on the single particle configuration by considering the difference between the moments of inertia of SD bands. To know which single particle orbits are involved in these SD bands, one has to calculate $J^{(2)}$ for that configuration and compare it with the experimental data.

The aim of the present work is to study the systematics of kinematic $J^{(1)}$ and dynamic moment of inertia $J^{(2)}$ of SD bands in the $A \sim 130$, 150, 190 mass regions in the framework of the N_pN_n scheme. This study may provide new insights into $J^{(1)}$ and $J^{(2)}$, which may be useful in studying the intrinsic structure of nuclei more clearly.

2 Theory

Several approaches are proposed to calculate the spin proposition of SD bands [31, 32]. The level spin for SD nuclei near the A$\sim$ 194 mass region was introduced by Becker et al. [33] in which transition energies of 25 SD bands of 13 nuclei were fitted by power- series expansion. The methods used to determine spins (I) associated with transitions in SD rotational bands in $A \sim 190$ region are given in Refs. [34–36]. Liu et al. [37] studied the variation of moments of inertia with angular momentum and also studied the systematics of bandhead moment of inertia. All the approaches are based upon the comparison of calculated transition energies or moments of inertia with their respective experimental results. Many authors [38–41] have calculated the transition energies for ND and SD bands, and also found their corresponding $J^{(1)}$ and $J^{(2)}$. Liu et al. [42] explained the turnover of the $J^{(2)}$ of the superdeformed nuclear state. Wu et al. [43] established the relation between $J^{(1)}$ and $J^{(2)}$ in SD nuclei. In the same year, Wu et al. [36] extracted $J^{(1)}$ and $J^{(2)}$ of SD bands from transition energies and discussed their variation with rotational frequency. One can extract the values of $J^{(1)}$ and $J^{(2)}$ by using the experimental intraband E2 transition energies from the tables of SD bands given by Singh et al. [44] and continuously updated data from Ref. [45]. The kinematic and dynamic moment of inertia is defined as;

$$J^{(1)}(I-1)/\hbar^2 = \frac{2I-1}{E_\gamma(I \to I-2)}, \tag{1}$$

$$J^{(2)}(I)/\hbar^2 = \frac{4}{E_\gamma(I+2 \to I) - E_\gamma(I \to I-2)}. \tag{2}$$

It is noted from the equations that $J^{(1)}$ depends upon the spin proposition whereas $J^{(2)}$ does not. To study the adiabatic invariant behaviour of dynamical moment of inertia $J^{(2)}$ of SD bands in the ^{194}Tl nucleus, Eq. (2) has

been applied [46]. It is also suggested in Ref [46] that $J^{(2)}$ is used to investigate the dependence of nuclear structure on the rotational frequency. The above-stated equations can also be useful in finding the band moment of inertia J_0 in different mass regions.

The phenomenon of high spin superdeformed rotational bands is specified by the kinematic moment of inertia $J^{(1)}$ and the dynamic moment of inertia $J^{(2)}$. To study the nuclear deformation, the estimation of valence nucleons is an important measure which can be studied in the framework of the $N_{\rm p}N_{\rm n}$ scheme. The formula given in Eq. (1) clearly states that the $J^{(1)}$ has a direct relation with spin. To study SD spectroscopy, the relation between spin and valence nucleons helps us to study phenomena like band termination [47], back bending [48], etc. In the phenomenon of band termination, as the spin increases, the valence nucleons pairs break and get realigned with the angular momentum of the nucleons orbiting along the rotational axis. This gives the nucleus a prolate shape. In the phenomena of back bending, the pairs of nucleons break as the spin increases the moment of inertia, and the nucleons go into different orbits. Therefore, both the quantities ($J^{(1)}$ and $N_{\rm p}N_{\rm n}$) can form a link with each other in terms of spin and valence nucleons.

The formula given in Eq. (2) clearly states that the $J^{(2)}$ is not related to the spin and is an important measure to study the SD bands. The study of SD bands depends upon the intruder orbitals [49], which have a strong effect on $J^{(2)}$. On the other hand, the $N_{\rm p}N_{\rm n}$ scheme [7] also plays an important role in studying the orbit dependence, shell gaps concept, and intruder orbitals, under the guidance of the p-n interaction. Therefore, both the quantities ($J^{(2)}$ and $N_{\rm p}N_{\rm n}$) can form a link with each other in terms of intruder orbitals.

The various valence nucleons with varied spin ranges can occupy different orbitals. Therefore, the nucleons polarize in several ways and many nuclear shapes can coexist based upon different configurations. The increasing number of protons and neutrons and increasing spin are characterized between the single particle shell effects and the collective degree of freedom. This leads to the different structural changes. The different types of structural change with spin and valence nucleons (valence nucleons and $J^{(1)}$) in different $A\sim$130, 150 and 190 mass regions are band termination, back bending, band mixing, band crossing, etc.

The structural changes can also be explained on the basis of intruder orbitals and valence nucleons (valence nucleons and $J^{(2)}$). In the $A\sim$130 mass region, the high j valence particle or the difference in the occupation of specific high N intruder orbitals, namely $h_{11/2}$, $d_{5/2}$, $g_{7/2}$, are mainly responsible for the structural changes. In the $A\sim$150 mass region, the different occupation of specific high N intruders, namely $j_{15/2}$ neutrons and $i_{13/2}$ protons, are mainly responsible for the structural changes. In the $A\sim$190 mass region, the quasiparticle alignment of the same high N intruders, namely $j_{15/2}$ neutrons and $i_{13/2}$ protons, are mainly responsible for the structural changes. The valence protons and neutrons together are expected to have strong and specific shape driving forces on the core of the superdeformed nucleus. Therefore phenomena like staggering and identical bands can be explained.

3 Results and discussion

The two attributes of SD bands that highlight their different rotational properties compared to the ND bands are large deformation and large shell gaps. The large deformation splits the j levels and hence contributes to reduced Coriolis interactions. In addition to this, large deformation alters the mean field potential and favours the nucleon states with high wavefunction density. The large shell gaps contributing to low−density states near the Fermi surface give rise to reduced pairing correlation strength. The large shell gap also highlights the stability against large changes in the deformation, as a function of spin [50]. The main factors that decide the behaviour of SD rotational bands are the single particle field, Coriolis and centrifugal forces, and the pairing correlations. The pairing correlations in different SD bands behave like rigid rotors at different angular momenta and moments of inertia (kinematic $J^{(1)}$ and dynamic moment of inertia $J^{(2)}$)[44, 45]. The $J^{(1)}$ and $J^{(2)}$ can be obtained by using experimental intraband E2 transition energies as stated in equation (1) and equation (2). The data have been taken from Ref.[44, 45]. The calculated values of kinematic and dynamic moment of inertia for the $A\sim$130, 150 and 190 mass regions are given in Tables 1 and 2.

3.1 Variation of $J^{(1)}$ with $N_{\rm p}N_{\rm n}$

The kinematic moment of inertia $J^{(1)}$ depends only upon spin. As the linking transitions are missing between SD bands and ND bands, features like exact excitation energies, spins and parities of the SD bands remain unknown. The $N_{\rm p}N_{\rm n}$ scheme is used to estimate the p-n interaction and helps in the evolution of nuclear deformation. A simple pattern is observed whenever nuclear data disclosing nuclear deformation is plotted against the $N_{\rm p}N_{\rm n}$ scheme.

In this work, the values of $J^{(1)}$ obtained with the help of the experimental intraband E2 transition energies formula as stated in equation (1) are plotted against $N_{\rm p}N_{\rm n}$. A complicated and irregular behaviour is observed in Figs. 1, 2 and 3 for the $A\sim$130, $A\sim$150 and $A\sim$190 mass regions. The irregular behaviour in the $A\sim$130 and

Table 1. The $J^{(1)}$ and $J^{(2)}$ values, in $\hbar^2\ MeV^{-1}$, for different SD bands in the $A\sim130$, 150 mass regions. The experimental data have been taken from Refs. [44, 45].

Z	N	SD BANDS	$J^{(1)}$	$J^{(2)}$
58	72	$^{130}Ce(1)$	32.37	32.78
58	72	$^{130}Ce(2)$	32.10	54.79
58	72	$^{130}Ce(3)$	29.86	55.55
58	72	$^{130}Ce(4)$	21.41	57.14
58	73	$^{131}Ce(1)$	54.14	56.33
58	73	$^{131}Ce(2)$	59.03	65.57
58	75	$^{133}Ce(1)$	61.49	65.57
58	75	$^{133}Ce(2)$	55.55	61.53
58	75	$^{133}Ce(3)$	50.15	137.93
59	73	$^{132}Pr(2)$	47.78	52.63
59	73	$^{132}Pr(1)$	41.66	57.97
59	73	$^{132}Pr(3)$	38.08	137.93
59	73	$^{132}Pr(4)$	47.55	57.97
59	74	$^{133}Pr(1)$	66.66	58.82
59	74	$^{133}Pr(2)$	67.5	56.33
59	74	$^{133}Pr(3)$	71.42	57.14
59	74	$^{133}Pr(4)$	70.64	62.5
60	72	$^{132}Nd(1)$	48.42	121.21
60	72	$^{132}Nd(2)$	46.98	153.84
60	72	$^{132}Nd(3)$	49.11	59.70
60	72	$^{132}Nd(4)$	48.34	80
61	72	$^{133}Pm(1)$	36.17	42.55
61	72	$^{133}Pm(2)$	35.50	41.23
64	86	$^{150}Gd(1)$	77.30	117.64
64	86	$^{150}Gd(14)$	72.92	80
64	86	$^{150}Gd(3)$	83.79	90.90
64	86	$^{150}Gd(13)$	74.92	117.64
64	86	$^{150}Gd(6)$	73.83	88.88
64	86	$^{150}Gd(11)$	83.33	83.33
64	86	$^{150}Gd(9)$	81.14	81.63
64	86	$^{150}Gd(10)$	83.33	85.10
65	86	$^{151}Tb(1)$	82.53	95.23
65	86	$^{151}Tb(2)$	86.37	90.90
65	86	$^{151}Tb(3)$	85.04	86.95
65	86	$^{151}Tb(4)$	85.82	85.01
65	86	$^{151}Tb(7)$	76.51	80.00
66	86	$^{152}Dy(1)$	84.71	86.95
66	86	$^{152}Dy(3)$	94.57	85.10
66	86	$^{152}Dy(4)$	85.07	78.43
66	86	$^{152}Dy(5)$	85.66	75.47
66	86	$^{152}Dy(6)$	85.30	93.02
64	87	$^{151}Gd(1)$	80.42	93.02
64	87	$^{151}Gd(2)$	79.88	95.23
64	87	$^{151}Gd(3)$	82.01	80.00
64	87	$^{151}Gd(4)$	81.63	97.56
64	87	$^{151}Gd(5)$	81.58	88.88
66	87	$^{153}Dy(1)$	91.53	88.88
66	87	$^{153}Dy(2)$	91.33	86.95
66	87	$^{153}Dy(3)$	91.16	86.95
66	87	$^{153}Dy(4)$	85.75	90.00
66	87	$^{153}Dy(5)$	91.52	85.01

Table 2. The $J^{(1)}$ and $J^{(2)}$ values, in $\hbar^2\ MeV^{-1}$, for different SD bands in the $A\sim150$, 190 mass regions. The experimental data have been taken from Refs. [44, 45].

Z	N	SD BANDS	$J^{(1)}$	$J^{(2)}$
65	86	$^{151}Tb(5)$	78.98	76.92
65	86	$^{151}Tb(6)$	78.48	78.43
64	87	$^{151}Gd(6)$	78.23	95.23
64	87	$^{151}Gd(2)$	79.88	95.23
81	114	$^{195}Tl(1)$	95.89	95.23
81	114	$^{195}Tl(2)$	95.23	100
81	113	$^{194}Tl(1)$	100.74	102.56
81	113	$^{194}Tl(2)$	100.47	102.56
81	113	$^{194}Tl(3)$	95.43	102.56
81	113	$^{194}Tl(4)$	95.45	102.56
81	112	$^{193}Tl(1)$	96.61	100
81	112	$^{193}Tl(2)$	96.91	97.56
81	112	$^{193}Tl(3)$	95.74	93.02
81	112	$^{193}Tl(4)$	103.58	97.56
81	111	$^{192}Tl(1)$	116.60	105.26
81	111	$^{192}Tl(2)$	115.38	108.10
81	111	$^{192}Tl(3)$	98.71	97.56
81	111	$^{192}Tl(4)$	98.59	97.56
81	110	$^{191}Tl(1)$	93.86	97.56
81	110	$^{191}Tl(2)$	94.59	97.56
81	108	$^{189}Tl(1)$	92.03	95.23
81	108	$^{189}Tl(2)$	91.80	100
80	115	$^{195}Hg(1)$	95.23	100
80	115	$^{195}Hg(2)$	94.89	100
80	115	$^{195}Hg(3)$	98.36	97.56
80	115	$^{195}Hg(4)$	99.41	102.56
80	114	$^{194}Hg(1)$	89.62	95.23
80	114	$^{194}Hg(3)$	94.59	100
80	114	$^{194}Hg(2)$	94.52	97.56
80	113	$^{193}Hg(1)$	94.42	97.56
80	113	$^{193}Hg(2)$	94.48	97.56
80	113	$^{193}Hg(3)$	94.01	97.56
80	113	$^{193}Hg(4)$	94.48	97.56
80	112	$^{192}Hg(1)$	88.78	90.90
80	112	$^{192}Hg(2)$	95.43	97.56
80	111	$^{191}Hg(1)$	109.32	97.56
80	111	$^{191}Hg(2)$	95.23	97.56
80	111	$^{191}Hg(3)$	95.58	97.56
80	111	$^{191}Hg(4)$	99.64	93.02
80	110	$^{190}Hg(1)$	85.17	93.02
80	110	$^{190}Hg(2)$	101.87	133.33
80	110	$^{190}Hg(3)$	111.11	102.56
79	112	$^{191}Au(1)$	117.6	95.23
79	112	$^{191}Au(2)$	95.47	102.56
79	112	$^{191}Au(3)$	93.99	105.26

$A\sim150$ mass regions may be due to the mixing of the bands (see Figs. 1 and 2). The band mixing may arise when the energy levels of SD bands with same parity and signatures are close to each other i.e. $E_{(1)}\approx E_{(2)}$ for I $\approx$ I_c. The different SD bands which get mixed with each other are ^{133}Ce(1), ^{131}Ce(1), ^{130}Ce(1), ^{132}Pr(2), ^{132}Nd(1),

and ^{133}Pm(1); ^{133}Ce(2), ^{131}Ce(2), ^{130}Ce(2), ^{132}Pr(1), ^{132}Nd(2), and ^{133}Pm(2); ^{133}Ce(3), ^{130}Ce(3), ^{132}Pr(3), and ^{132}Nd(3); and ^{130}Ce(4), ^{132}Pr(4), and ^{132}Nd(4) (see Fig. 1).

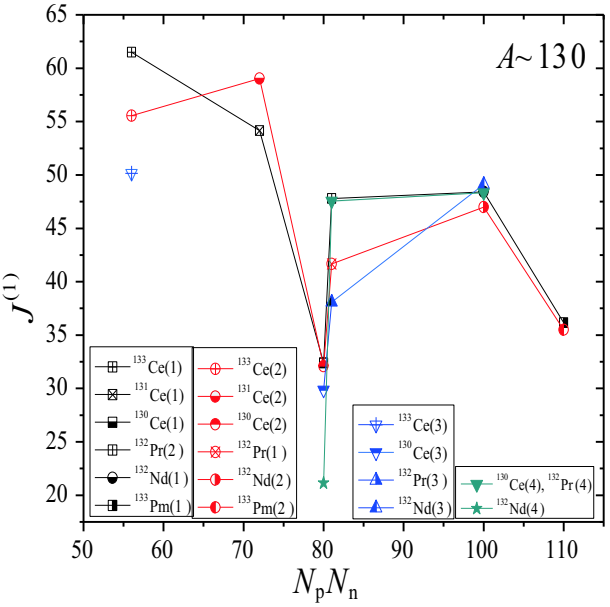

Fig. 1. Variation of kinematic moment of inertia $J^{(1)}$ versus N_pN_n in the $A\sim130$ mass region.

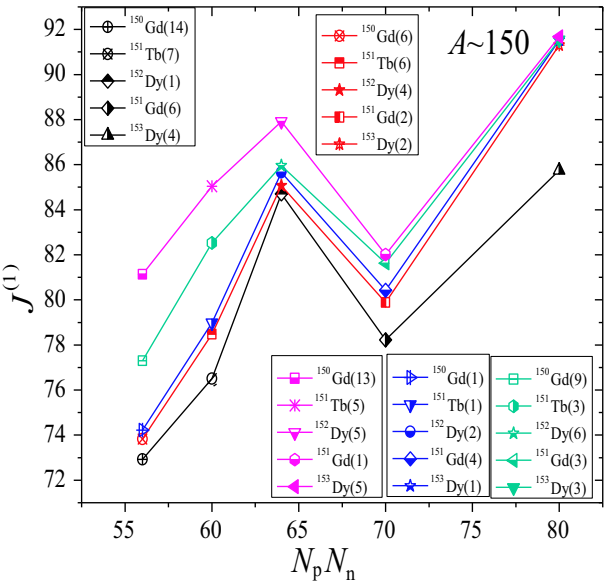

Fig. 2. Variation of kinematic moment of inertia $J^{(1)}$ versus N_pN_n in the $A\sim150$ mass region.

In Fig. 2, the SD bands get mixed with each other are ^{150}Gd(14), ^{151}Tb(7), ^{152}Dy(1), ^{151}Gd(6), and ^{153}Dy(4); ^{150}Gd(6), ^{151}Tb(6), ^{152}Dy(4), ^{151}Gd(2), and ^{153}Dy(2); ^{150}Gd(13), ^{151}Tb(5), ^{152}Dy(5), ^{151}Gd(1), and ^{153}Dy(5); ^{150}Gd(1), ^{151}Tb(1), ^{152}Dy(2), ^{151}Gd(4), and ^{153}Dy(1); and ^{150}Gd(9), ^{151}Tb(3), ^{152}Dy(6), ^{151}Gd(3), and ^{153}Dy(3). All the above-stated SD bands of the $A\sim130$, A~150 mass regions can serve as examples of band mixing. The another possible reason is that the spin of the lowest level observed in the SD bands in the $A\sim130$ and $A\sim150$ regions is usually high, which further indicates band mixing. In the $A\sim190$ mass region, most of the bands cross each other, as shown in Fig. 3. Band crossing occurs when signatures split SD rotational bands into two families, $I=j$ and $I=j+1$, each consisting of levels differing in spin by $2\hbar$. Therefore the $I=j$ sequence is shifted downwards in energy (called the favored signature) against the other (called the unfavored signature). Therefore, as the spin increases, they cross each other. The different SD bands which participate in band crossing are Tl, Hg and Au (see Fig. 3). These SD bands can serve examples of band crossing. As a result of the band mixing and band crossing, a reliable spin measurement is difficult to achieve in these mass regions.

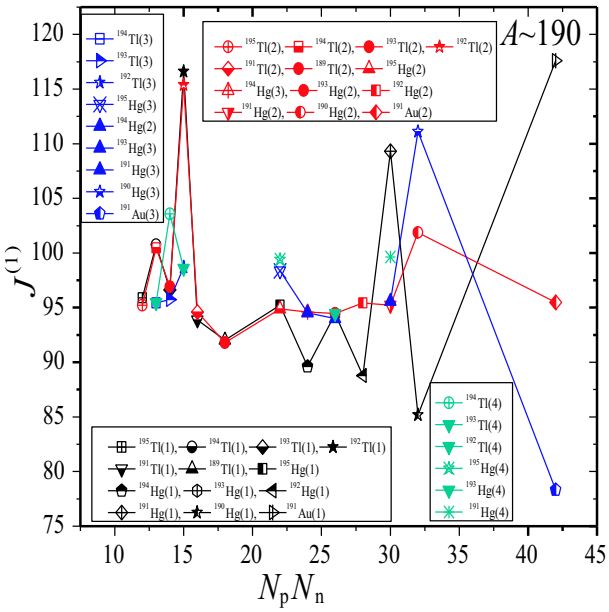

Fig. 3. Variation of kinematic moment of inertia $J^{(1)}$ versus N_pN_n in the $A\sim190$ mass region.

3.2 Variation of $J^{(2)}$ with N_pN_n

We have calculated the dynamic moment of inertia $J^{(2)}$ for all the SD bands in the $A\sim130$, 150 and 190 mass regions by using experimental intraband E2 transition energies. We have plotted the dynamic moment of inertia versus N_pN_n as shown in Figs. 4, 5, and 6, and found that $J^{(2)}$ versus N_pN_n shows a staggering behaviour in the $A\sim130$, 150 and 190 mass regions.

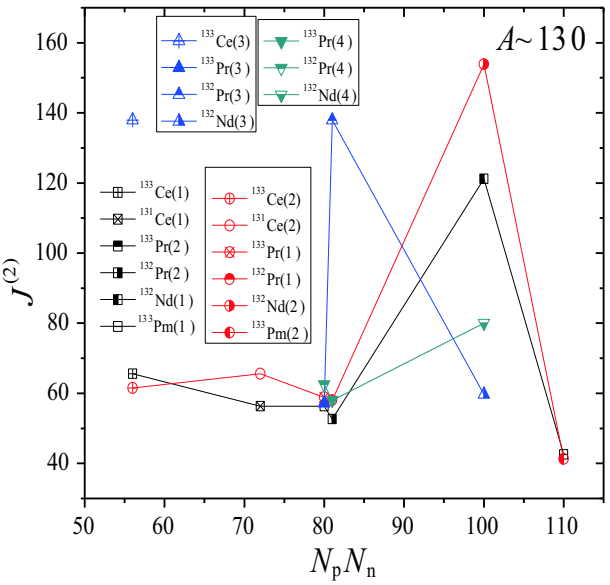

Fig. 4. Variation of dynamic moment of inertia $J^{(2)}$ versus N_pN_n in the $A\sim130$ mass region.

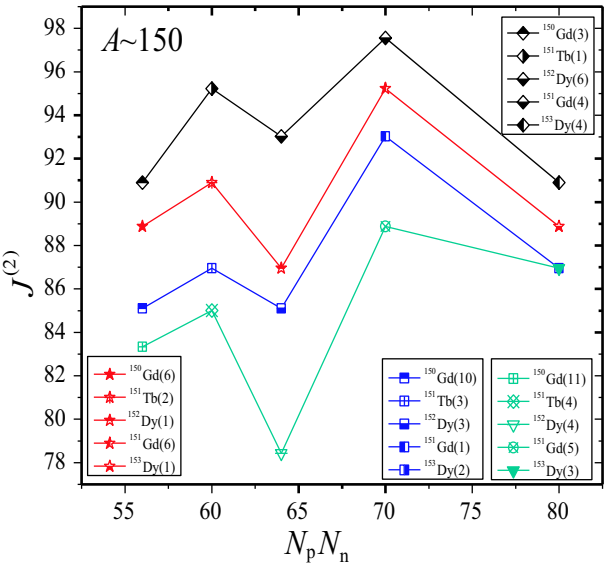

Fig. 5. Variation of dynamic moment of inertia $J^{(2)}$ versus N_pN_n in the $A\sim150$ mass region.

The staggering may occur due to Coriolis mixing, which causes the two sequences to decouple, so levels in one band are pushed up in energy with respect to the other. This behaviour is known in the literature as $\triangle$ I=2 bifurcation. The presence of bifurcation has been examined in the $A\sim130$ [51], $A\sim190$ [52], and A~150 [53, 54] regions. From Figs. 4, 5 and 6, the different SD bands of the $A\sim130$, 150, 190 mass regions participate in staggering behaviour. The SD nuclei resulting in staggering in the $A\sim130$ mass region are ^{133}Ce, ^{131}Ce, ^{133}Pr, ^{132}Pr, ^{132}Nd, and ^{133}Pm (see Fig. 4).

In the A~150 mass region, ^{150}Gd, ^{151}Tb, ^{152}Tb, ^{151}Gd, and ^{153}Dy are the SD nuclei participating to form a zigzag pattern (see Fig. 5). Similarly, ^{195}Hg, ^{194}Hg, ^{193}Hg, ^{192}Hg, ^{191}Hg, ^{190}Hg, ^{189}Hg, ^{195}Tl, ^{194}Tl, ^{193}Tl, ^{192}Tl, ^{191}Tl, ^{190}Tl, ^{189}Tl and ^{191}Au are some SD nuclei forming the zigzag pattern in the $A\sim190$ mass region (see Fig. 6). The other probable reason for staggering may be the occupation of high j intruder orbitals and intrinsic hexadecapole moments of specific single particle states. These both play a vital role in generating the zigzag pattern [55, 56].

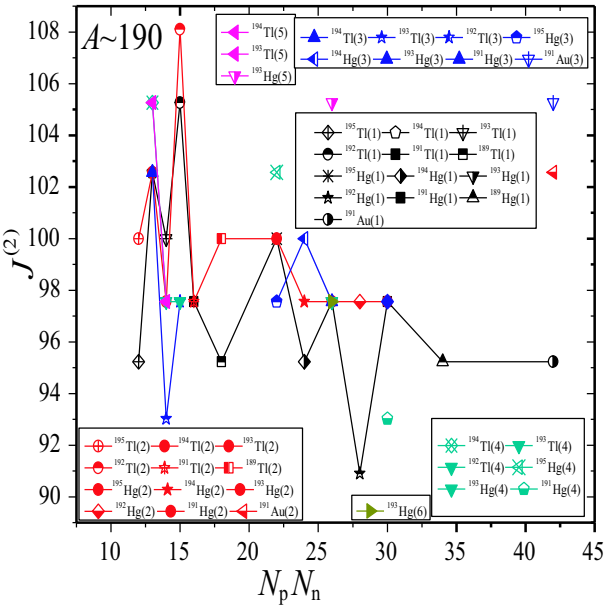

Fig. 6. Variation of dynamic moment of inertia $J^{(2)}$ versus N_pN_n in the $A\sim190$ mass region.

4 Conclusion

In this work, we have calculated $J^{(1)}$ and $J^{(2)}$ for SD bands in the $A\sim130$, 150, 190 mass regions by using experimental intraband E2 transition energies and presented their systematics with the N_pN_n scheme. The superdeformed rotational bands can be described by using $J^{(1)}$ and $J^{(2)}$. In general, $J^{(1)}$ and $J^{(2)}$ are used for nucleus characterization. We have plotted the variation of kinematic moment of inertia $J^{(1)}$ versus N_pN_n, and observed band mixing in the $A\sim130$, 150 mass regions, and band crossing in the $A\sim190$ mass region. Due to the band mixing and band crossing in these mass regions, spin determination remains unpredictable. We have also plotted the variation of dynamic moment of inertia $J^{(2)}$ with N_pN_n, and it is highly interesting to observe the staggering behaviour in the $A\sim130$, 150, 190 mass regions.

References

1 A. de Shalit and M. Goldhaber, Phys. Rev., **92**: 1211 (1953)
2 I. Talmi, Rev. Mod. Phys. **34**: 704 (1962)
3 P. Federman and S. Pittel, Phys. Lett. B, **69**: 385 (1977)
4 P. Federman and S. Pittel, Phys. Lett. B, **77**: 29 (1978)
5 P. Federman and S. Pittel, Phys. Rev. C, **20**: 820 (1979)
6 P. Federman and R. Campos, Phys. Lett. B, **82**: 9 (1979)
7 R. F. Casten, Nucl. Phys. A, **443**: 1 (1985)
8 R. F. Casten, Phys. Rev. Lett., **54**: 1991 (1985)
9 R. F. Casten and N. V. Zamfir, J. Phys. G, **22**: 1521 (1996)
10 R. F. Casten, D. S. Brenner, and P. E. Haustein, Phys. Rev. Lett., **58**: 658 (1987)
11 R. F. Casten, Phys. Lett. B, **152**: 145 (1985)
12 J. Y. Zhang, R. F. Casten, and D. S. Brenner Phys. Lett. B, **227**: 1 (1989)
13 J. B. Gupta, H. M. Mittal, J. H. Hamilton, and A. V. Ramayya, Phys. Rev. C, **42**: 1373 (1990)
14 J. B. Gupta, H. M. Mittal, and S. Sharma, Phys. Scr., **41**: 660 (1990)
15 J. B. Gupta, A. K. Kavathekar, and R. Sharma, Phys. Scr., **51**: 316 (1995)
16 T. S. Saini and J. B. Gupta, Proc. DAE Symp. Nucl. Phys., **56**: 332 (2011)
17 J. B. Gupta and A. K. Kavathekar, Phys. Scr., **56**: 574 (1997)
18 Y. M. Zhao, R. F. Casten, and A. Arima, Phys. Rev. Lett, **85**: 720 (2000)
19 Y. M. Zhao and A. Arima, Phys. Rev. C, **68**: 017301 (2003)
20 G. Jin, J. H. Yoon, and D. Cha, J. Phys. G: Nucl. Part. Phys., **35**: 035105 (2008)
21 Y. Byun, G. Jin, J. H. Yoon, and D. Cha, J. Korean Phys. Soc, **54**: 792 (2009)
22 G. J. Fu, H. Jiang, Y. M. Zhao, and A. Arima, Phys. Rev. C, **82**: 014307 (2010)
23 P. Kumari and H. M. Mittal, International Journal of Modern Phys. E, **24**: 1550033 (2015)
24 H. M. Mittal and N. Sharma, Armenian Journal of Phys., **5**: 165–175 (2012)
25 N. Sharma and H. M. Mittal, International Journal of Modern Phys. E, **22**: 1350053 (2013)
26 C. Rigollet, P. Bonche, H. Flocard et al, Phys. Rev. C, **59**: 3120 (1999)
27 Y. Lei, C. Lin, and J. Zeng, **40**: 652–657 (1997)
28 W. Nazarwicz, R. Wyss, and A. Johnson, Nucl. Phys. A, **503**: 285 (1989)
29 M. A. Riley et al, Nucl. Phys. A, **512**: 178 (1990)
30 M. A. Bentley, Proc. of Fourth Int. Summer School, 78–90 (1991)
31 R. Piepenbring and K. V. Protasov, Z. Phys. A, **345**: 7 (1993)
32 I. Ragnarsson, Nucl. Phys. A, **557**: 167 (1993)
33 J. A. Becker, E. A. Henry, A. Kuhnert, T. F. Wang, and S. W. Yates, Phys. Rev. C, **46**: 889 (1992)
34 J. G. Drapper et al, Phys. Rev. C, **42**: R1791 (1990)
35 J. Y. Zeng, J. Meng, C. S. Wu, E. G. Zhao, Z. Xing, and X. Q. Chen, Phys. Rev. C, **44**: R1745 (1991)
36 C. S. Wu, J. Y. Zeng, Z. Xing, X. Q. Chen, and J. Meng, Phys. Rev. C, **45**: 261 (1992)
37 S. X. Liu and J. Y. Zeng, Phys. Rev. C, **58**: 3266 (1998)
38 A. Bohr and B. R. Mottelson, *Nuclear Structure* (Benjamin, New York, 1975), Vol. 2 Chap.4
39 S. M. Harris, Phys. Rev. Lett., **13**: 663 (1964); Phys. Rev. A, **509**: 138 (1965)
40 P. Holmberg and P. O. Lipas, Nucl. Phys. A, **117**: 552 (1968)
41 C. S. Wu and J. Y. Zeng, Commun. Theor. Phys. (Beijing), **8**: 51 (1987)
42 Y. Liu, J. Song, H. Z. Sun, J. J. Wang, and E. G. Zhao, Phys. G: Nucl. Part. Phys., **24**: 117–124 (1998)
43 C. S. Wu, L. Cheng, C. Z. Lin, and J. Y. Zeng, Phys. Rev. C, **45**: 2507 (1992)
44 B. Singh, R. Zywina, and R. B. Firestone, Nuclear Data Sheets, **97**: 241–592 (2002)
45 http://www.nndc.bnl.gov/
46 H. M. Mittal and N. Sharma, Journal of Phys.: Conference Series, **420**: 012056 (2013)
47 Deleplanque et al, Phys. Rev. C, **52**: R2302 (1995)
48 S. Lunardi et al, Phys. Rev. Lett. **72**: 1427 (1994)
49 T. Bengtsson et al, Phys. Lett. B, **208**: 39 (1988)
50 D. Ward and P. Fallon, Advance in Nuclear Physics, **26**: 229 (2001)
51 A. T. Semple et al, Phys. Rev. Lett., **76**: 3671 (1996)
52 B. Cederwall et al, Phys. Rev. Lett., **72**: 3150 (1994)
53 S. Flibotte et al, Phys. Rev. Lett., **71**: 4299 (1993)
54 L. Bernstein et al, Phys. Rev. C, **52**: R1171 (1995)
55 F. Donau et al, Phys. Lett. B, **387**: 667 (1996)
56 I. M. Pavlichenkov, Phys. Rev. C, **55**: 1275 (1997)